Urbanization-Induced Increases in Heavy Precipitation are Magnified by Moist Heatwaves in an Urban Agglomeration of East China

CHENXI LI,[a] XIHUI GU,[a,b,c,d,e] LOUISE J. SLATER,[f] JIANYU LIU,[g] JIANFENG LI,[h] XIANG ZHANG,[i] AND DONGDONG KONG[a,c]

[a] *Department of Atmospheric Science, School of Environmental Studies, China University of Geosciences, Wuhan, China*
[b] *State Key Laboratory of Water Resources and Hydropower Engineering Science, Wuhan University, Wuhan, China*
[c] *Centre for Severe Weather and Climate and Hydro-Geological Hazards, Wuhan, China*
[d] *Hubei Key Laboratory of Yangtze Catchment Environmental Aquatic Science, Wuhan, China*
[e] *State Environmental Protection Key Laboratory of Source Apportionment and Control of Aquatic Pollution, Ministry of Ecology and Environment, Wuhan, China*
[f] *School of Geography and the Environment, University of Oxford, Oxford, United Kingdom*
[g] *Hubei Key Laboratory of Critical Zone Evolution, School of Geography and Information Engineering, China University of Geosciences, Wuhan, China*
[h] *Department of Geography, Hong Kong Baptist University, Hong Kong, China*
[i] *National Engineering Research Center of Geographic Information System, School of Geography and Information Engineering, China University of Geosciences, Wuhan, China*

(Manuscript received 1 April 2022, in final form 27 September 2022)

ABSTRACT: Heavy precipitation (HP) events can be preceded by moist heatwaves (HWs; i.e., hot and humid weather), and both can be intensified by urbanization. However, the effect of moist HWs on increasing urban HP remains unknown. Based on statistical analyses of daily weather observations and ERA5 reanalysis data, we herein investigate the effect of moist HWs on urban-intensified HP by dividing summer HP events into NoHW- and HW-preceded events in the Yangtze River delta (YRD) urban agglomeration of China. During the period 1961–2019, the YRD has experienced more frequent, longer-lasting, and stronger intense HP events in the summer season (i.e., June–August), and urbanization has contributed to these increases (by 22.66%–37.50%). In contrast, urban effects on HP are almost absent if we remove HW-preceded HP events from all HP events. Our results show that urbanization-induced increases in HP are associated with, and magnified by, moist HWs in urban areas of the YRD region. Moist HWs are conducive to an unstable atmosphere and stormy weather, and they also enhance urban heat island intensity, driving increases in HP over urban areas.

SIGNIFICANCE STATEMENT: The contribution of urbanization to increases in heavy precipitation has been widely reported in previous studies. HP events can be preceded by moist heatwaves (hot and humid extremes); however, it is unknown whether moist HWs enhance urban effects on HP. We choose the Yangtze River delta urban agglomeration to explore this question and find that urbanization contributes to the increasing frequency, duration, maximum intensity, and cumulative intensity of HP events in the summer season. However, this urban signal is not detectable if we remove HW-preceded events from all HP events. In other words, moist HWs play a key role in magnifying urbanization-induced increases in HP. Given that urban areas are projected to continue expanding and moist HWs are projected to occur with increasing frequency and intensity in the future, the role of HWs in the urban water cycle merits further investigation.

KEYWORDS: Extreme events; Climate change; Urban meteorology

1. Introduction

In the last decade, major cities have experienced sequential occurrences of unprecedented heatwaves (HWs) and devastating rainstorms, such as the events that occurred on 29 June 2012 in Washington, D.C., United States, and on 10 July 2017 in Paris, France. The succession of different extremes within several days, that is, a rainstorm preceded by a HW, may cause much greater damages than separate events alone and are thus receiving more and more attention (Wang et al. 2019; Zhang and Villarini 2020; Chen et al. 2021; Liao et al. 2021; You and Wang 2021; Wu et al. 2021; Gu et al. 2022; Li et al. 2022). For example, more than 30% of flood events in the central United States during 1979–2017 were preceded by heat stress, and this percentage is larger in the case of greater floods (Zhang and Villarini 2020). Similarly, China has experienced on average 26% of HWs followed by heavy precipitation (HP) in the warm season (i.e., May–September) of 1981–2005 and these HW-preceded HP events are projected to occur with greater frequency and intensity by the end of the twenty-first century (You and Wang 2021). Both studies indicated a lagged connection between HWs and HP; that is, HWs can provide

Supplemental information related to this paper is available at the Journals Online website: https://doi.org/10.1175/JCLI-D-22-0223.s1.

Corresponding authors: Xihui Gu, guxh@cug.edu.cn; Dongdong Kong, kongdongdong@cug.edu.cn

DOI: 10.1175/JCLI-D-22-0223.1

favorable large-scale environmental conditions for HP formation.

In cities, urbanization plays a key role in the development of the large-scale environmental conditions associated with HP events (P. Yang et al. 2017; Wang et al. 2018; W. Zhang et al. 2018; Gu et al. 2019a,b; Y. Li et al. 2020, 2021; Song et al. 2021; Yu et al. 2022) as well as HWs (X. Yang et al. 2017; Liao et al. 2018; Luo and Lau 2018; Kong et al. 2020). HWs bring high air temperature, which can enhance the atmospheric water-holding capacity following the Clausius–Clapeyron equation (Giorgi et al. 2011; Dai et al. 2018; Ali et al. 2021; C. X. Li et al. 2021). During moist HWs, the specific humidity accumulates in the lower troposphere, which can increase the precipitable water (Zhang and Villarini 2020). Both the heat and high humidity jointly result in atmospheric instability [e.g., greater convective available potential energy (CAPE)] and high values of moisture convergence (Zhang and Villarini 2020; You and Wang 2021), promoting HP formation. Urbanization has been shown to increase rainstorms through similar mechanisms by enhancing surface sensible heat flux in urban areas relative to their rural surroundings. The urban heat island (UHI) effect can thermally drive changes in circulation patterns, enhancing vertical uplift and moisture convergence (Freitag et al. 2018; Yang et al. 2019; Li et al. 2020). Given that urbanization can enhance HWs (Wouters et al. 2017; Liao et al. 2018; Luo and Lau 2018; Kong et al. 2020) and some HWs may trigger HP events, we hypothesize that HWs may play an important role in amplifying the urban effects on rainstorms.

Here, we explore this hypothesis by comparing the frequency, duration, maximum, and cumulative intensity of HP events preceded and not preceded by moist HWs (i.e., HW-preceded and NoHW-preceded HP events) in the Yangtze River delta (YRD), a typical highly urbanized region in eastern China. The YRD is experiencing longer-lasting, more frequent, and more intense HWs and heat stress in urban than rural areas (Liao et al. 2018; Luo and Lau 2018; Kong et al. 2020), and urbanization has been shown to increase HP markedly in this region (Jiang et al. 2020; Jie Wang et al. 2021; Liang and Ding 2017; Yu et al. 2022). To our knowledge, this is the first study investigating the role of HWs in urbanization-induced increases in rainstorms. This investigation aims to provide a deeper understanding of the impacts of urbanization on HP and novel insights into a new type of compound extremes: the successive occurrence of HWs and HP events in cities.

2. Data and methods

a. Data

The YRD region includes 27 cities and a total area of 301 700 km^2 accounting for 2.2% of China, while it contributes 11% of population and 25% of gross domestic product. Along with the rapid development of the economy and the population growth, the YRD is experiencing a remarkable urbanization process, which has been shown to affect local climate (Lu et al. 2019; Luo and Lau 2019; Jiang et al. 2020; Jie Wang et al. 2021). Daily precipitation, near-surface air temperature, and near-surface relative humidity time series collected at 115 stations across the YRD were obtained from the National Meteorological Science Data Center (Fig. 1). These data cover the period of 1961–2019 and are quality controlled and homogenized before they are released. Because we focus on HWs and HP events, only values in summer (i.e., June–August) are used. The June–August observed data are more than 99.5% complete in all 115 stations during the period 1961–2019, with only a few missing values in most stations (Fig. S1 in the online supplemental material).

Annual land-use/land-cover (LULC) data at 30-m spatial resolution during the period 1980–2015 were produced by Xu et al. (2020). These data divide LULC into six first-level categories [i.e., cropland, forest, grassland, water body, built-up areas (i.e., urban areas), and unused land] and provide percentages of each category in each 1-km pixel (Xu et al. 2020).

We obtained hourly air temperature (at 550–1000 hPa; °C), specific humidity (at 550–1000 hPa; g kg^{-1}), U component of wind (at 550–1000 hPa; m s^{-1}), V component of wind (at 550–1000 hPa; m s^{-1}), vertical velocity (at 550–1000 hPa; Pa s^{-1}), CAPE (J kg^{-1}), surface net longwave radiation flux (W m^{-2}), surface net shortwave radiation flux (W m^{-2}), surface sensible and latent heat flux (W m^{-2}), and total column water vapor (i.e., integrated water vapor; kg m^{-2}) from the ERA5 reanalysis data (Hersbach et al. 2020). CAPE is a single-level variable and an indication of the instability (or stability) of the atmosphere (higher CAPE value indicates that the atmosphere may become more unstable; Tan and Gan 2017; You and Wang 2021). The ERA5 reanalysis data cover the period 1961–2019 and have a spatial resolution of 0.25°. Hourly values are aggregated into daily values in this study.

The ERA5 reanalysis dataset is produced using the Integrated Forecasting System (IFS) Cy41r2, which does not contain sophisticated urban parameterizations (Hersbach et al. 2020). A few studies queried the ability of the ERA5 to simulate urban effects in urban areas (Nogueira et al. 2022; Zhang et al. 2022). For example, Nogueira et al. (2022) found that the ERA5 cannot capture the UHI effect in Paris, France, during 2004–18 due to lacking urban processes in the IFS Cy41r2 and its relatively coarse spatial resolution. However, a mass of observations (from stations, satellites, radars, etc.) are assimilated in the ERA5 reanalysis dataset, and the state-of-the-art data assimilation technologies (such as 4D-Var) significantly improve the quality of the ERA5 simulations (Hersbach et al. 2020). The assimilated observations and improved accuracy to reproduce observations could make the ERA5 implicitly include urban effects (Bassett et al. 2021; Venter et al. 2021; Meili et al. 2022; Yu et al. 2022). Meili et al. (2022) identified the diurnal and seasonal patterns of urban dry islands at global scale based on observations and the ERA5 reanalysis dataset. At local scale, Bassett et al. (2021) used the ERA5 reanalysis data to estimate the long-term changes in UHI intensity in London, United Kingdom, during 1950–2019. In our study region, Yu et al. (2022) employed the ERA5 reanalysis dataset (such as the K index, an indicator representing atmospheric instability) to explore the mechanisms behind

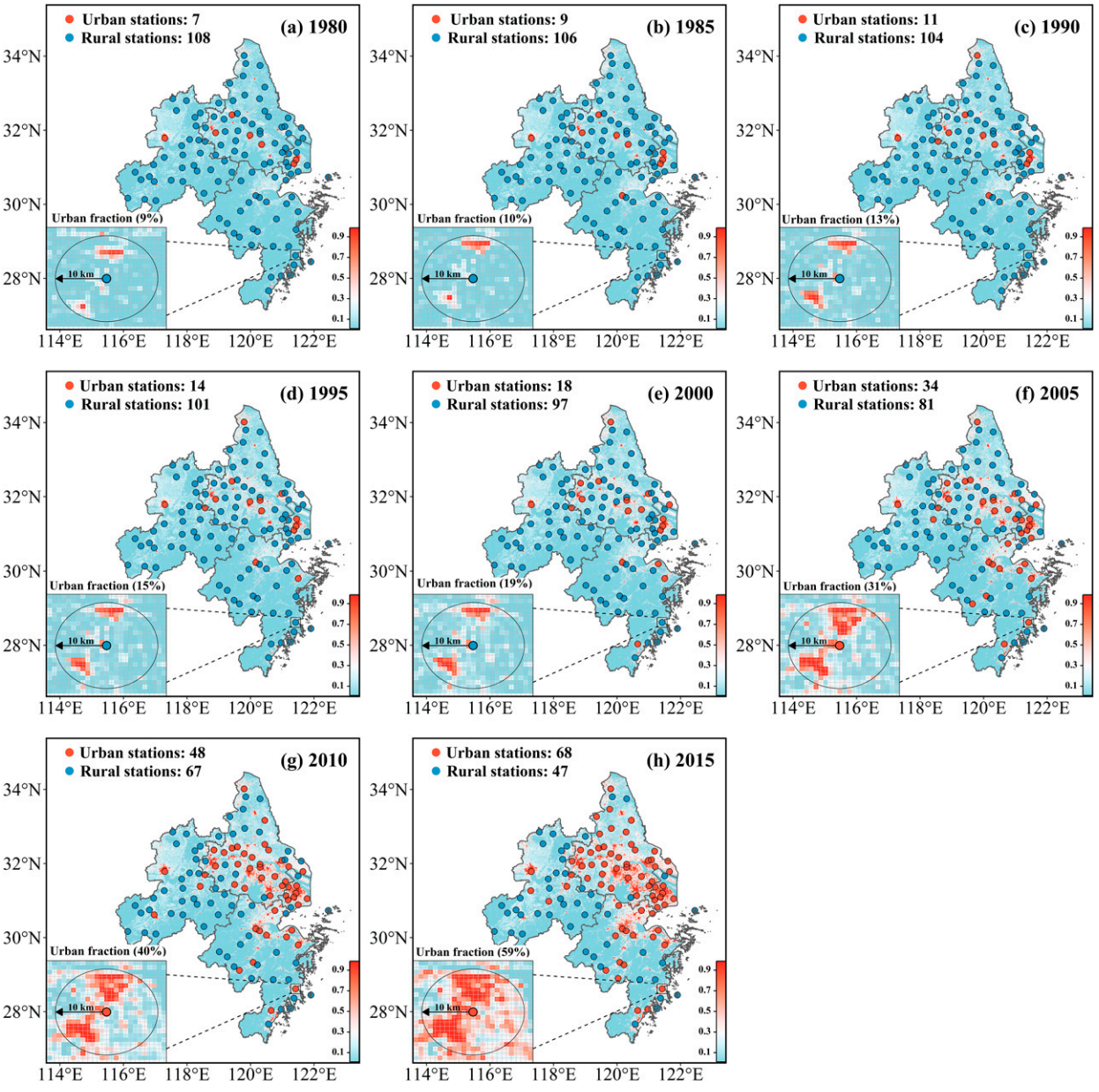

FIG. 1. Ratio of built-up areas to total area in each 1 km × 1 km grid from the years 1980 to 2015 over the YRD. The annual built-up areas are obtained from the LULC data with a 1-km resolution during the period 1980–2015 (Xu et al. 2020). Color bars indicate the ratio of built-up areas in each 1 km × 1 km grid, blue (red) points are rural (urban) stations identified in the corresponding year, and the circular buffers in the bottom left of each panel provide an example of a station, which was identified as (a)–(e) rural (urban fraction < 30%) and then (f)–(h) urban (urban fraction ≥ 30%). Urban fraction is the percentage of built-up areas in the 10-km buffer.

the urban effects on heavy precipitation in the YRD. These studies enhance our confidence that the ERA5 could capture the urban effects in the YRD region.

b. Identification of HW-preceded HP events

Moist HWs are identified based on the daily heat index, which considers both near-surface air temperature and relative humidity, and is calculated using the Rothfusz regression (Li et al. 2018; Kong et al. 2020):

$$\begin{aligned} \mathrm{HI} = {} & -8.7847 + 1.6114 \times \mathrm{SAT} - 0.012\,308 \times \mathrm{SAT}^2 + \mathrm{RH} \\ & \times (2.3385 - 0.146\,12 \times \mathrm{SAT} + 2.2117 \times 10^{-3} \\ & \times \mathrm{SAT}^2) + \mathrm{RH}^2 \times (-0.016\,425 + 7.2546 \\ & \times 10^{-4} \times \mathrm{SAT} - 3.582 \times 10^{-6}\mathrm{SAT}^2), \end{aligned} \tag{1}$$

where the variables are defined as the heat index (HI; °C), near-surface air temperature (SAT; °C), and near-surface relative humidity (RH; %). This equation should be adjusted

(please see more details available at https://www.wpc.ncep.noaa.gov/html/heatindex_equation.shtml) if the following conditions occur: RH $<$ 13% and 26.67°C $<$ SAT $<$ 44.4°C; RH $>$ 85% and 26.67°C $<$ SAT $<$ 30.56°C or estimated HI value is less than 26.67°C. Here, daily SAT and RH values are the station-based observations at the 115 stations across the YRD region (Fig. 1).

As mentioned in the introduction, the amplification effects of urbanization on HP are associated with the UHI (i.e., higher temperature in urban areas than the surrounding rural areas; W. Zhang et al. 2018; Yang et al. 2021; Yu et al. 2022). The synergistic interactions between UHI and HWs have been widely reported in previous studies, that is, the UHI is intensified under HWs (Li and Bou-Zeid 2013; Li et al. 2015; Zong et al. 2021). HWs may play an important role in the amplification effects of urbanization on HP, given the relations between HWs, UHI, and HP. On the other hand, heat stress (associated with high air temperature and atmospheric humidity) has been found likely to trigger HP events in central United States (Zhang and Villarini 2020) and in China (Li et al. 2022). The heat index is a widely used indicator to assess the heat stress (e.g., Fischer and Schar 2010; Li et al. 2018), and urbanization contributes to the substantial increases in magnitude and frequency of heat stress based on the heat index in China during the past decades (Luo and Lau 2018, 2021; Wang et al. 2021; Kong et al. 2020). Under given RH (SAT), higher SAT (RH) leads to a larger heat index; moreover, in comparison with other indices of heat stress (such as wet-bulb temperature), the heat index increases faster than SAT (Li et al. 2018; Luo and Lau 2018; Li et al. 2022). Therefore, the heat index is suitable to effectively reflect the synergies between UHI and HWs. The heat index used to identify moist HWs based on near-surface air temperature and relative humidity seems rather more suited for human biometeorological studies than for precipitation-related studies. In fact, for the urban impacts on precipitation, an index quantifying boundary layer–integrated heat and moisture might be more appropriate and could lead to even more clear signals. This could eventually be explored in future studies.

For each calendar day of June–August in each station, the 90th percentile of heat index values in 450 days during the climatological period 1961–90 (7 days prior and posterior to the calendar day sampled from each year; i.e., 15 days per year during the 30 years) is calculated as the threshold. All heat index values above this threshold are identified and consecutive days no less than 3 days are taken as a HW event (X. Yang et al. 2017; Luo and Lau 2018).

Daily precipitation observations at the 115 stations are used to identify HP events. We take the 90th percentile of all June–August wet days (daily precipitation exceeding 0.1 mm) of the climatological period 1961–90 as the threshold (within the range 23.71–49.64 mm for the 115 stations in this study) and then identify the values above this threshold as HP days. Any consecutive HP days are taken as one HP event. In the same way, a second sample of HP events is also identified by taking 50 mm as the threshold. We then calculate annual statistics: frequency (annual number of HP events), duration (annual number of HP days), maximum intensity (annual maximum daily precipitation above the threshold; i.e., maximum value of daily precipitation minus the threshold) in HP days, and cumulative intensity (total annual precipitation above the threshold; i.e., total amount of daily precipitation minus the threshold) on all HP days. Trends in these annual statistics are estimated by using the nonparametric modified Mann–Kendall method (Hamed and Rao 1998).

If a HW event occurs within 3 days prior to a HP event, we identify this as a HW-preceded HP event, otherwise, this is a NoHW-preceded HP event. This identification is consistent with previous studies, where different time windows (i.e., 1, 5, and 7 days) were tested and found to have little influence on the identification results of HW-preceded HP events (Zhang and Villarini 2020; Chen et al. 2021; You and Wang 2021; Li et al. 2022). In this study, all HP events, NoHW-preceded HP events, and HW-preceded HP events are identified using in situ observations at the 115 stations.

c. *Identification of urban stations*

For each of the 115 stations, we establish a n-km circular buffer (see Fig. 1 for an example) to identify urban and rural stations, which is consistent with previous studies (Liao et al. 2018; Tysa et al. 2019; Wang et al. 2021, 2022; Yu et al. 2022). If the percentage of built-up areas to total buffer area exceeds 30% (this percentage is consistent with previous studies; X. Yang et al. 2017; Liao et al. 2018; Luo and Lau 2019; Yu et al. 2022) in any year of the period 1980–2015 (the period of LULC data availability), then the station is identified as an urban station, otherwise, it is a rural station. The annual built-up areas in each 1 $\times$ 1 km^2 grid during 1980–2015 are obtained from the LULC data (Xu et al. 2020). The optimal buffer radius is selected based on the Spearman correlations between trends in annual HP characteristics (i.e., frequency, duration, maximum intensity, and cumulative intensity) and urban expansion rates (Fig. 2). Specifically, for each of the 115 stations, annual built-up areas in the n-km circular buffer around this station are counted during the period 1980–2015, and the urban expansion rate is estimated as the trend of annual built-up areas (using the nonparametric modified Mann–Kendall method; Hamed and Rao 1998). In a n-km buffer around the 115 stations, we can obtain 115 urban expansion rates in this n-km buffer. In section 2b, we can obtain a total of 115 trend values in one of the four HP characteristics at the 115 stations during the period 1961–2019. Taking the 1-km buffer and the frequency of HP events as an example, we estimate the Spearman correlation between the 115 urban expansion rates and the 115 trend values in HP frequency. We repeat this process for the buffer with a radius from 1 to 20 km and the four HP characteristics (Fig. 2). The optimal radius is set as 10 km because the correlations are significant at 0.05 significance level and tend to remain stable beyond a 10-km radius. Following this procedure, 68 (47) stations are identified as urban (rural) stations (Fig. 1h).

In general, there are two pathways to identify urban stations: based on constant and dynamic LULC data, respectively (Liao et al. 2018; Tysa et al. 2019; Wang et al. 2021, 2022; Yu et al. 2022). For example, Tysa et al. (2019) only employed the LULC data in the year 2015 to identify urban and

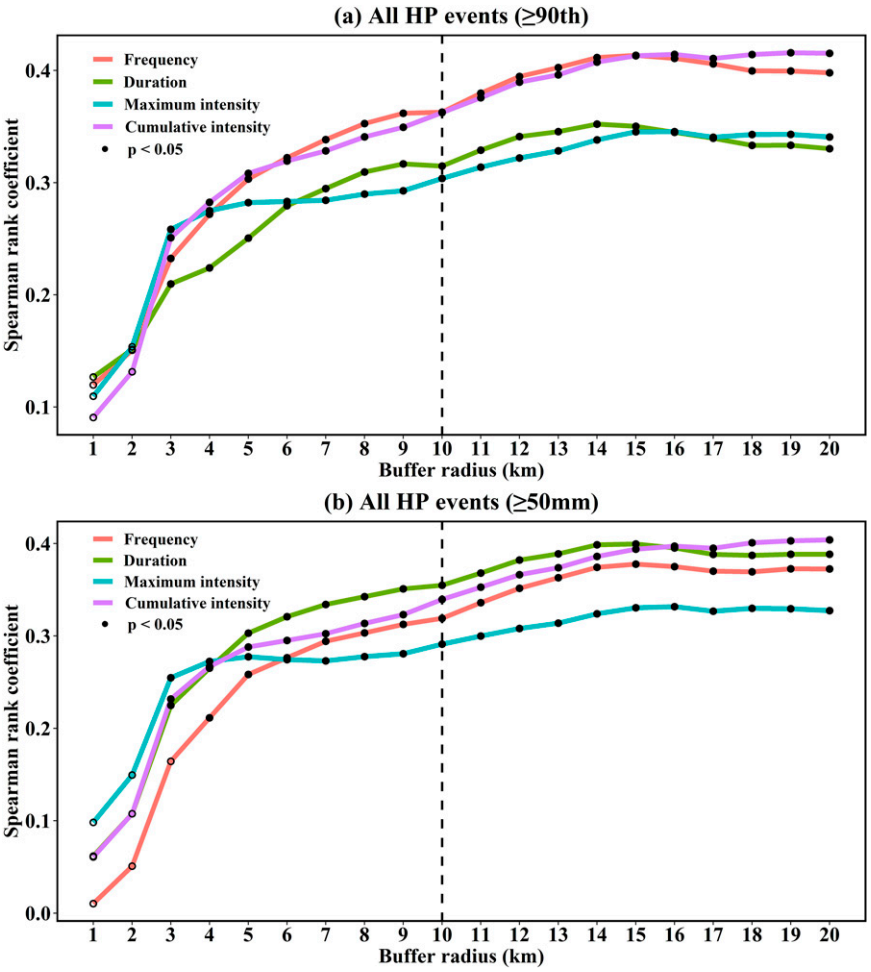

FIG. 2. Spearman correlations between trends in annual characteristics (i.e., frequency, duration, maximum intensity, and cumulative intensity) of all HP events during the summer season (i.e., June–August) of 1961–2019 and urban expansion rates in the *n*-km buffer of each of the 115 stations during the period 1980–2015 over the YRD. The HP events are identified by using the (a) 90th percentile of wet days (daily precipitation above 0.1 mm) and (b) 50 mm as the threshold, respectively (see section 2b). All HP events are identified using in situ daily observations at the 115 stations across the YRD. A *n*-km (from 1 to 20 km) buffer of each of the 115 stations is built to count the annual built-up areas in this buffer during the period 1980–2015 based on the LULC data. For a station, the urban expansion rate is the trend of annual built-up areas in the *n*-km buffer during the period 1980–2015.

rural stations and evaluated urban effects in regional temperature series in China during 1980–2015. More studies dynamically classified urban and rural stations based on time-varying LULC data (X. Yang et al. 2017; Liao et al. 2018; Luo and Lau 2019; Shi et al. 2021; Wang et al. 2021, 2022; Yu et al. 2022). For example, Wang et al. (2021) identified urban stations based on the 1980, 1990, 1995, 2000, 2005, and 2010 LULC data and quantified the urban impacts on compound hot extremes in China's cities during 1961–2014; using a similar way to identify urban stations, Wang et al. (2022) estimated contributions of urbanization to the declining atmospheric humidity in China during 1971–2017. All these studies defined urban stations as those with built-up areas in the buffer centered on this station exceeding a given percentage in any year of having LULC data. In these studies and our study, some urban stations transfer from rural stations during the identification period (i.e., 1980–2015 in our study). Our previous study classified the transitional stations as urbanizing stations and found a consistent amplification effect of urbanization on heavy precipitation in the YRD region during 1961–2019 no matter how urbanizing stations were separated from or merged into urban stations (Yu et al. 2022).

d. Estimation of urban effect and contribution

The UHI intensity is defined as the difference in near-surface air temperature between an urban area and its surrounding

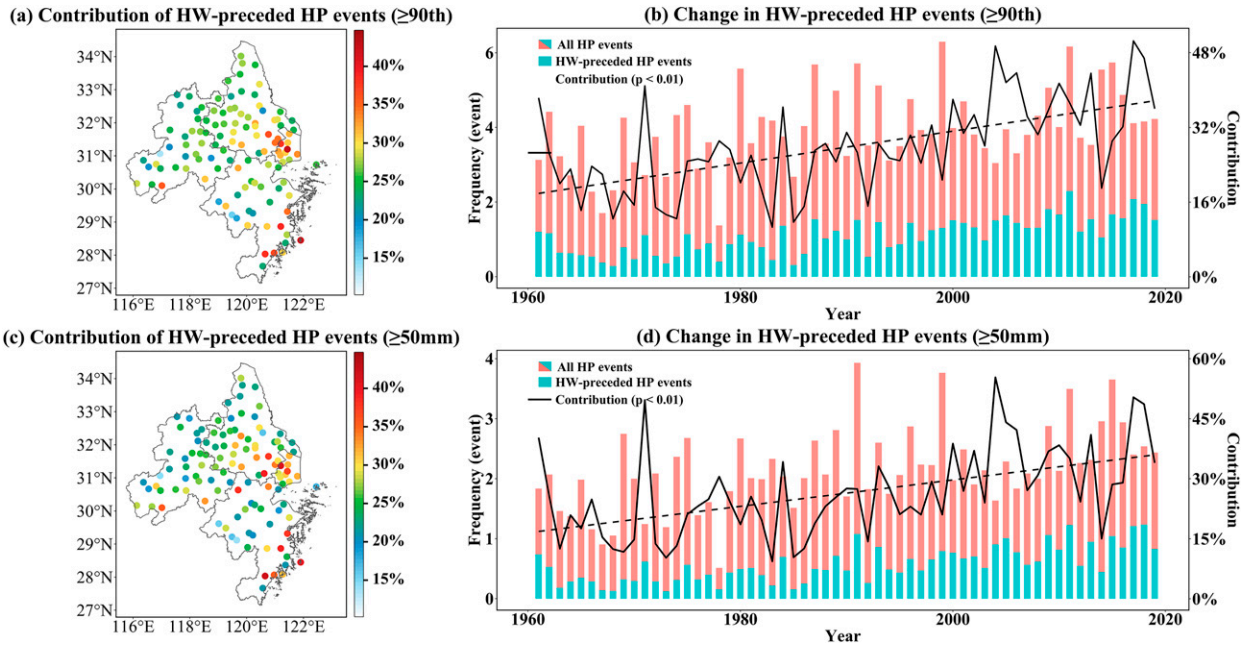

FIG. 3. Fractional contribution of HW-preceded HP events (HWs within a 3-day window prior to a HP event) to all HP events during the summer season of 1961–2019 over the YRD. All HP events and HW-preceded HP events are identified using in situ daily observations at the 115 stations across the YRD. For each of the 115 stations, the fractional contribution is the ratio of HW-preceded HP events to all HP events. The HP events are identified by using the (a),(b) 90th percentile of wet days (daily precipitation above 0.1 mm) and (c),(d) 50 mm as the threshold, respectively. The spatial distribution of the fractional contributions is shown in (a) and (c). In (b) and (d), the red (blue) bar plots show regional average frequency of all (HW preceded) HP events, the black solid lines are the annual fractional contribution of HW-preceded HP events (i.e., the value of blue bar divided by the value of red bar), and the dashed lines are the corresponding linear trends.

rural areas, which is similar to previous studies (e.g., Zhao et al. 2021; Qian et al. 2022). Annual characteristics (frequency, duration, maximum intensity, and cumulative intensity) of HP events for all the urban (rural) stations across the YRD region are regionally averaged to obtain regional mean time series during the period 1961–2019. Trends in regional mean time series of the four HP characteristics for urban (rural) stations are estimated using the nonparametric modified Mann–Kendall method (Hamed and Rao 1998), respectively. The difference in the trends in regional mean time series of the four HP characteristics between urban and rural stations is taken as urban effect (UE). Then, the urban contribution (UC) to HP is estimated as the ratio of UE to trends in the regional mean time series of the four HP characteristics for urban stations. These estimations of UE and UC are based on in situ observations at the 115 stations and are similar to previous studies quantifying UE and UC for temperature (Luo and Lau 2018; Ren et al. 2008).

3. Results and discussion

a. *Long-term changes in HW-preceded and NoHW-preceded HP events*

During the summer season of 1961–2019, the YRD on regional average experienced 3.92 (2.15) HP events per year taking the 90th percentile (50 mm) as the threshold, and 27.71% (26.74%) of these events were preceded by HWs occurring within 3 days (Fig. 3). You and Wang (2021) also found a consistent percentage of HWs followed by HP events in the YRD and indicated that the high CAPE, low convective inhibition, and strong vertically integrated moisture convergence occurring after the end of HWs enhanced convection and stormy weather. The frequency of HW-preceded HP events for all stations pooled together shows a significantly increasing trend as a rate of 0.20/0.12 event per decade (i.e., 18.63% and 21.43% per decade; the linear trend divided by the average frequency of HW-preceded HP events during 1961–2019). This increasing trend is also found in the annual fractional contribution of HW-preceded events to total HP events ($p < 0.05$). The substantial increase of HW-preceded HP events warns of the growing risk of such compound events in the YRD. We also notice that the stations with larger contributions of HW-preceded HP events are mainly concentrated in areas with rapid urbanization (i.e., eastern YRD; see Figs. 1 and 3a,c), implying that HWs in urban areas may have a higher likelihood of being followed by HP events. Due to the consistent behaviors of HW-preceded HP events when using the two thresholds of 90th percentile and 50 mm (Fig. 3), the following analyses are based only on the 90th percentile threshold.

We divide all HP events into HW-preceded and NoHW-preceded events and first explore the spatial distributions of trends in their frequency, duration, maximum intensity, and cumulative intensity (Fig. 4). The YRD is dominated by increasing trends in these HP characteristics (Figs. 4a–d). More

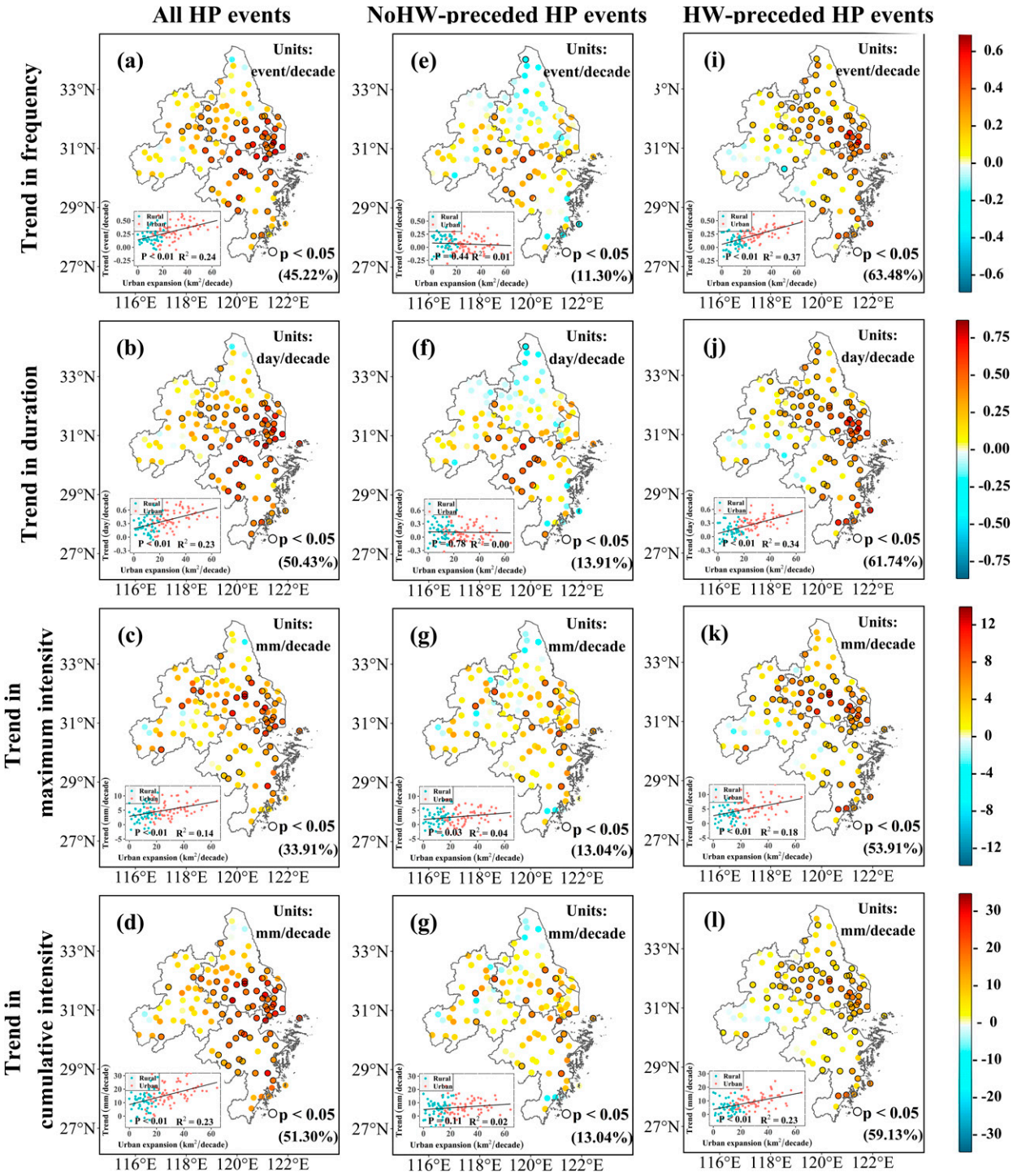

FIG. 4. Maps showing trends in the annual characteristics (frequency, duration, maximum intensity, and cumulative intensity) of (a)–(d) all HP events, (e)–(h) NoHW-preceded HP events (i.e., HP events not preceded by moist HW), and (i)–(l) HW-preceded HP events across the YRD during the summer season of 1961–2019. All HP events, NoHW-preceded HP events, and HW-preceded HP events are identified using in situ daily observations at the 115 stations across the YRD. Each colored dot represents one station, dots with black outlines indicate that trends in the annual characteristics of HP events are significant at the 95% confidence level, and the percentage of stations with significant trends to all the 115 stations is indicated in parentheses in the bottom right of each panel. Inset scatterplots in each panel show linear regressions between the trends in annual HP characteristics during the summer season of 1961–2019 and urban expansion rates during the period 1980–2015. For each of the 115 stations, urban expansion rate is estimated as the trend of annual built-up areas in the 10-km buffer around this station. The annual built-up areas are obtained from the LULC data with a 1-km resolution during the period 1980–2015. In the scatterplots, blue (red) dots indicate rural (urban) stations.

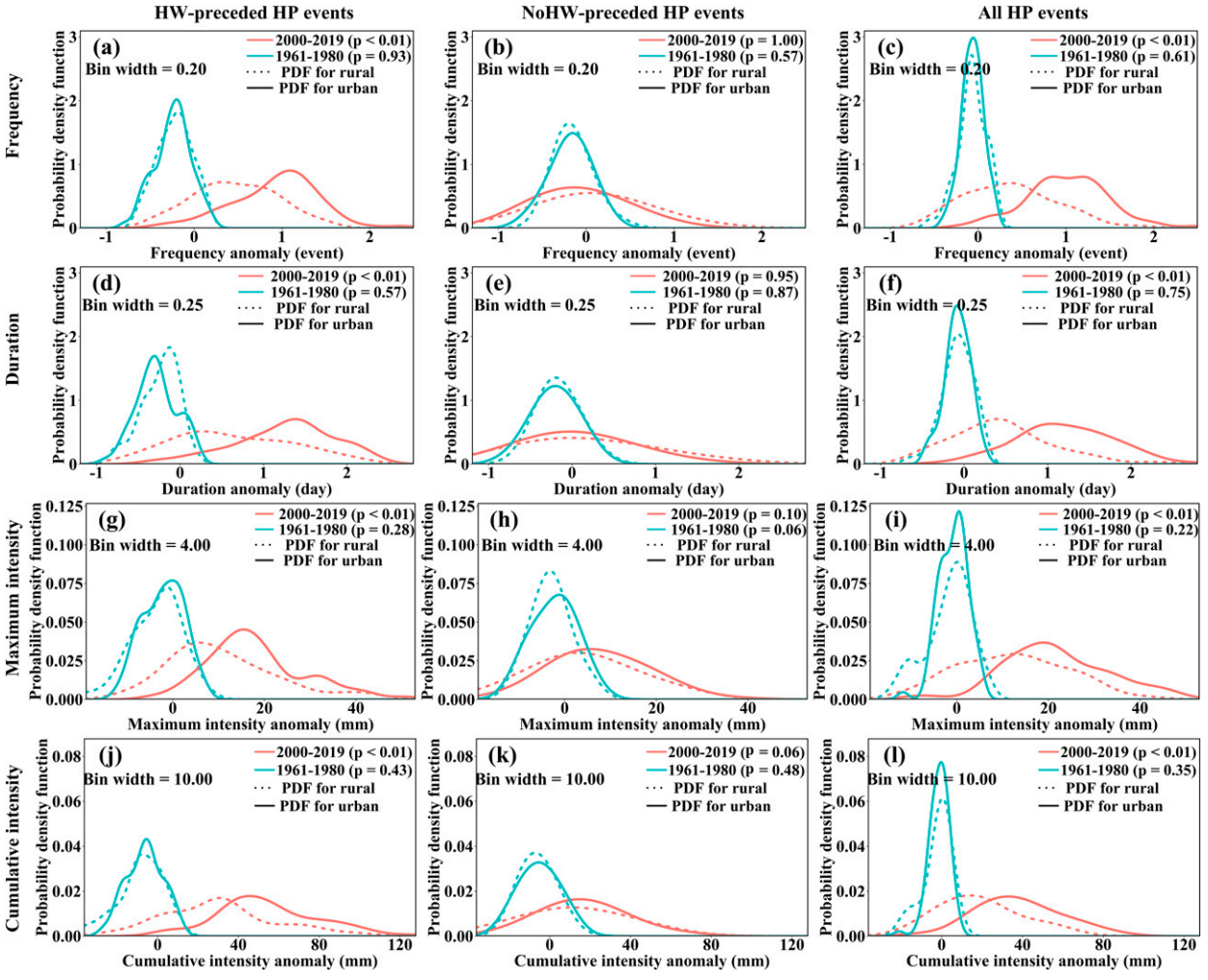

FIG. 5. PDFs of anomalies of annual frequency, duration, maximum intensity, and cumulative intensity of all, HW-preceded, and NoHW-preceded HP events between 68 urban and 47 rural stations (see Fig. 1h for their locations) over the YRD. All HP events, NoHW-preceded HP events, and HW-preceded HP events are identified using in situ daily observations at the 115 stations across the YRD. The anomalies are calculated relative to the climatological period 1961–90, and anomalies are plotted for the less/more urbanized period (i.e., 1961–80/2000–19). The significance of the differences in PDFs between urban and rural stations is tested by using the Kolmogorov–Smirnov method (Massey 1951; Mazdiyasni and AghaKouchak 2015).

frequent, longer-lasting, and more intense HP events are found in the areas that have experienced widespread urbanization (e.g., eastern YRD), which is also confirmed by the significant positive relations between trends in all four HP characteristics and urban expansion rates (see scatterplots in Figs. 4a–d). These results indicate that urbanization contributes to the increases in HP events (and their characteristics) over the YRD, which is also widely reported in previous studies (Jiang et al. 2020; Jie Wang et al. 2021; Liang and Ding 2017). However, the amplification effects of urbanization on HP are only found in HW-preceded HP events (Figs. 4e–h) and are very weak/absent from in NoHW-preceded ones (Figs. 4i–l). Specifically, there is high consistency in the spatial distribution of trends in the frequency, duration, maximum intensity, and cumulative intensity of all HP events and HW-preceded HP events. Increases in the four indices of HW-preceded HP events are most prominent in stations with high urban expansion rates, but this relation is not seen in NoHW-preceded HP events (see scatterplots in Figs. 4e–l).

We also compare the probability density function (PDF) of the anomalies of frequency, duration, maximum intensity, and cumulative intensity of all, HW-preceded, and NoHW-preceded HP events between urban and rural stations, respectively (Fig. 5). The anomalies are calculated relative to the climatological period 1961–90, and we plot the PDFs during the less (more) urbanized period [i.e., 1961–80 (2000–19)]. During the less urbanized period, no differences in the PDFs (i.e., $p > 0.05$) between urban and rural stations are observed in the four indices as well as all, HW-preceded, and NoHW-preceded HP events. In contrast, both urban and rural stations have experienced a shift toward

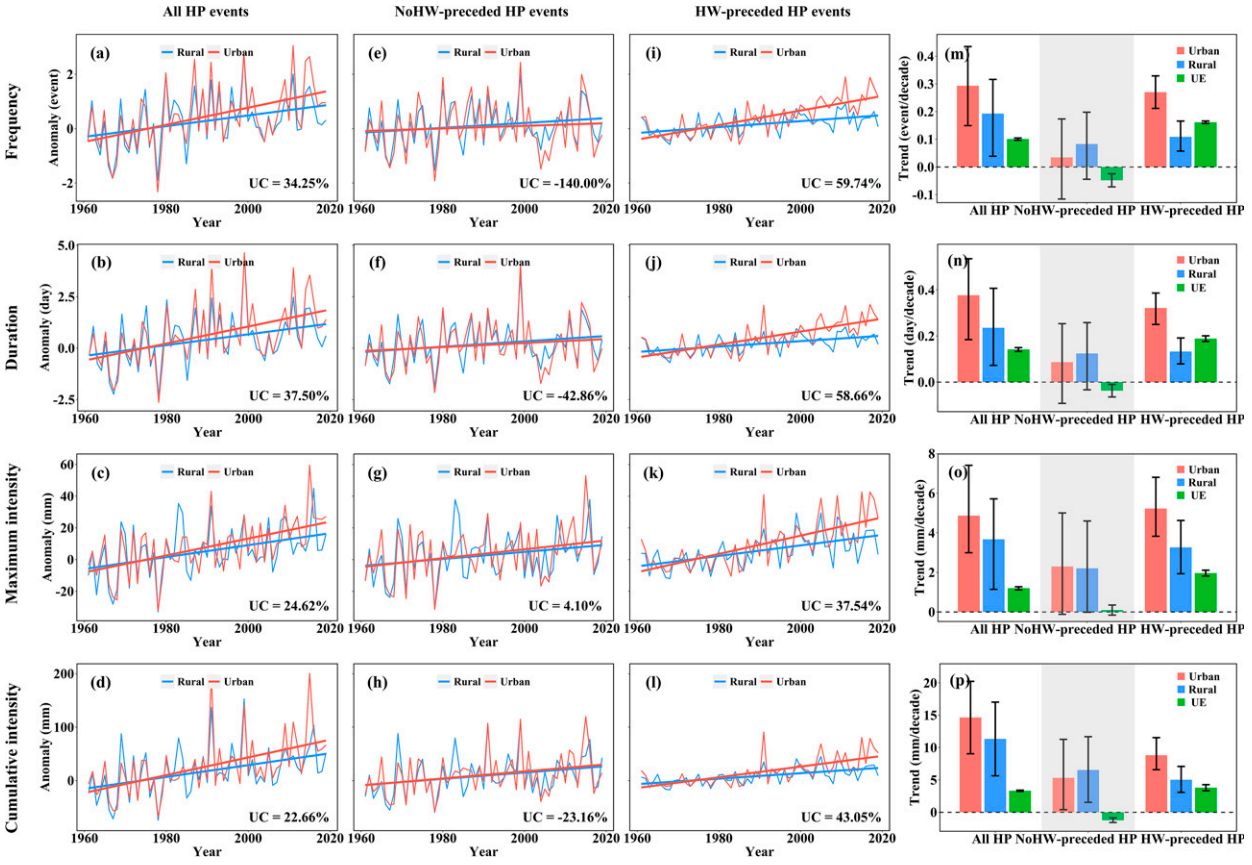

FIG. 6. Differences between urban and rural stations of trends in the annual characteristics (frequency, duration, maximum intensity, and cumulative intensity) of (a)–(d) all HP events, (e)–(h) NoHW-preceded HP events, and (i)–(l) HW-preceded HP events during the summer season of 1961–2019. All HP events, NoHW-preceded HP events, and HW-preceded HP events are identified using in situ daily observations at the 115 stations across the YRD. The irregular blue (red) lines in (a)–(l) indicate time series of the mean HP characteristics from all 47 rural (68 urban) stations over the YRD during the summer season of 1961–2019, and the corresponding straight blue (red) lines are their linear trends. UC in (a)–(l) indicates contribution of urbanization to these trends in urban areas. In (m)–(p), blue (red) bar plots indicate the linear trends in rural (urban) areas, green bar plots indicate UE (differences between urban and rural trends), and error bars are their 25%–75% confidence intervals obtained by bootstrapping.

more frequent, longer-lasting, and stronger HP events since 2000 (see the rightward shifts in these PDFs during the period 2000–19). These increases in HP events in both urban and rural stations have been attributed to anthropogenic climate change (Lu et al. 2020; Chen and Sun 2017; Ma et al. 2017). However, larger urban–rural differences are evident in the more urbanized period, that is, the PDFs for urban stations show farther rightward shifts and considerably larger tails than that for rural stations. This urban–rural contrast ($p < 0.01$) is observed for all HP events and for HW-preceded HP events. However, there are still no differences in the urban/rural PDFs ($p > 0.05$) of NoHW-preceded HP events in the recent 20-yr period. These findings suggest that HWs play a key role in urbanization-induced increases in the four HP characteristics.

Overall, during the past six decades, the YRD has experienced 47.32% (30.05%), 53.73% (34.27%), 58.42% (39.92%), and 84.72% (55.20%) of increases in frequency, duration, maximum intensity, and cumulative intensity of HP events in urban (rural) areas (Figs. 6a–d). The corresponding contributions of urbanization are estimated as 34.25%, 37.50%, 24.62%, and 22.66%. For HW-preceded HP events, much faster increases in these four indices are found in urban than rural areas (Figs. 6i–l), and the contributions of urbanization are even higher for HW-preceded events than for all HP events (i.e., 59.74%, 58.66%, 37.54%, and 43.05%). However, there are no differences in the trends of the four indices of NoHW-preceded HP events between urban and rural stations (Figs. 6e–h). Additionally, positive urban effects are not observed in NoHW-preceded HP events but are found in all and HW-preceded HP events (Figs. 6m–p). The urban effects are even higher in HW-preceded than all HP events. These results confirm that moist HWs magnify urbanization-induced increases in the four HP characteristics. This finding is not altered when altering the buffer radius from 1 to 20 km and the percentage of built-up areas from 20% to −50% within the buffer to identify urban stations (Figs. S2 and S3).

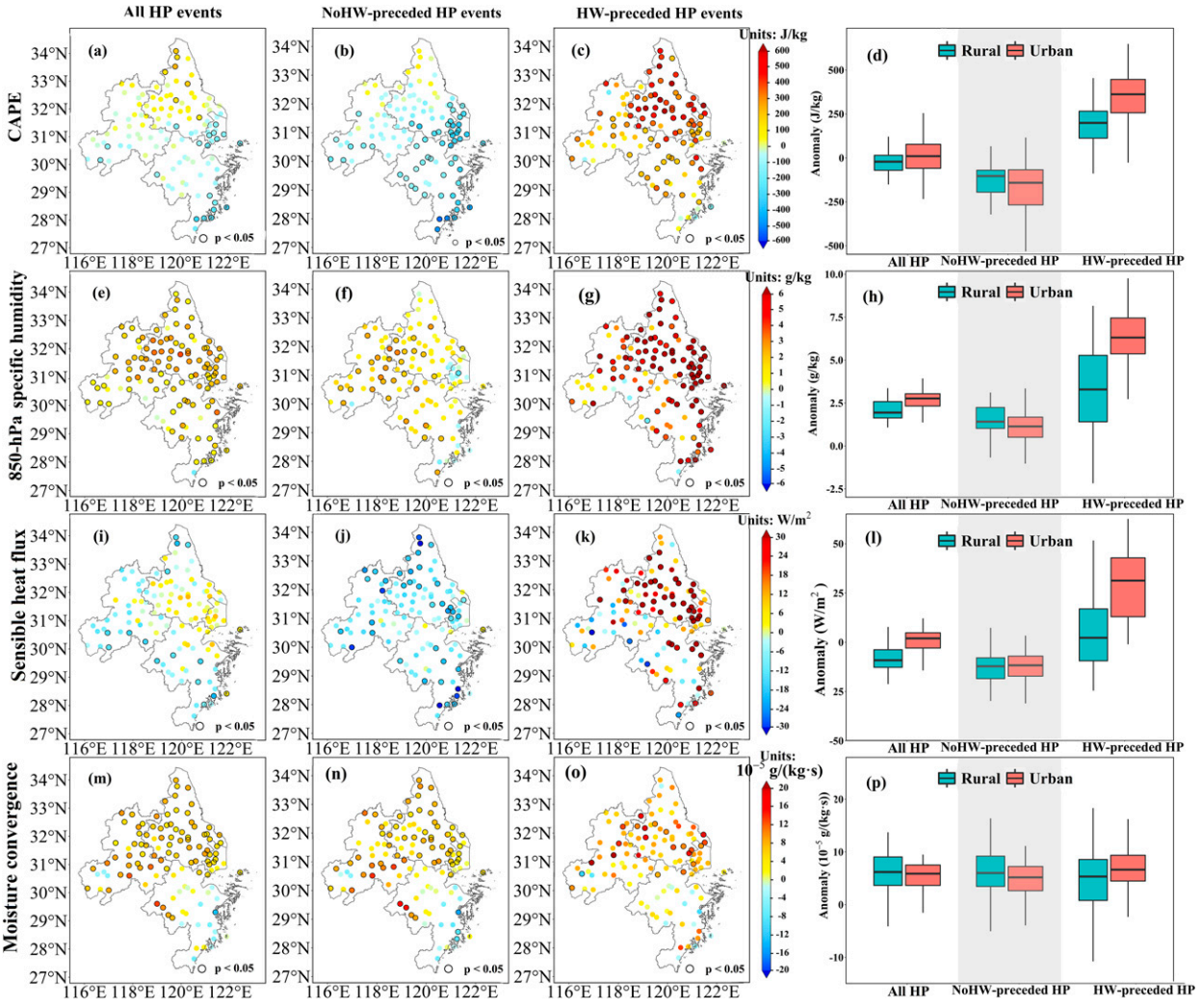

FIG. 7. Composite anomalies of CAPE, 850-hPa specific humidity, surface sensible heat flux, and 850-hPa moisture convergence obtained from the ERA5 reanalysis data in the one day prior to all, NoHW-preceded, and HW-preceded HP events, respectively, during the summer season of 1961–2019 over the YRD. All HP events, NoHW-preceded HP events, and HW-preceded HP events are identified using in situ daily observations at the 115 stations across the YRD. If one of the 115 stations is located at an ERA5 grid, we match daily values of CAPE, 850-hPa specific humidity, surface sensible heat flux, and 850-hPa moisture convergence in this ERA5 grid with this station. The anomalies are differences of values in the 1 day prior to HP events relative to the climatological summer mean during the period 1961–90; in the three left columns, the difference in the stations with black outlines is significant at the 95% confidence level. Boxplots for the anomalies at 68 urban and 47 rural stations (see Fig. 1h for their locations), respectively, are shown on the right.

b. *Possible mechanisms of moisture HWs magnifying increases in urban HP*

As suggested in previous studies, HWs can provide favorable large-scale environmental conditions before the occurrence of HP events (Zhang and Villarini 2020; You and Wang 2021; Wang et al. 2019). We first diagnose the differences in composite anomalies of CAPE, 850-hPa specific humidity, surface sensible heat flux, and 850-hPa moisture convergence in the lower atmosphere in the 1, 2, and 3 day(s) prior to all, HW-preceded, and NoHW-preceded HP events relative to climatological summer mean, respectively (Fig. 7 and Figs. S4, S5). Among the three categories, positive anomalies of CAPE, specific humidity, surface sensible heat flux, and moisture convergence are the most prominent for HW-preceded HP events, with the highest values located over urban areas. This is also the case when comparing values of these large-scale environmental variables in the 1, 2, and 3 day(s) prior to HW-preceded HP events with those from NoHW-preceded events (Fig. S6). During consecutive HW–HP events, moist HWs enhance surface sensible heat flux, accumulate atmospheric moisture, and then increase atmospheric instability and strengthen moisture convergence. These HW-driven synoptic preconditions prior to HP events are clearly stronger in urban areas, indicating the synergistic effects

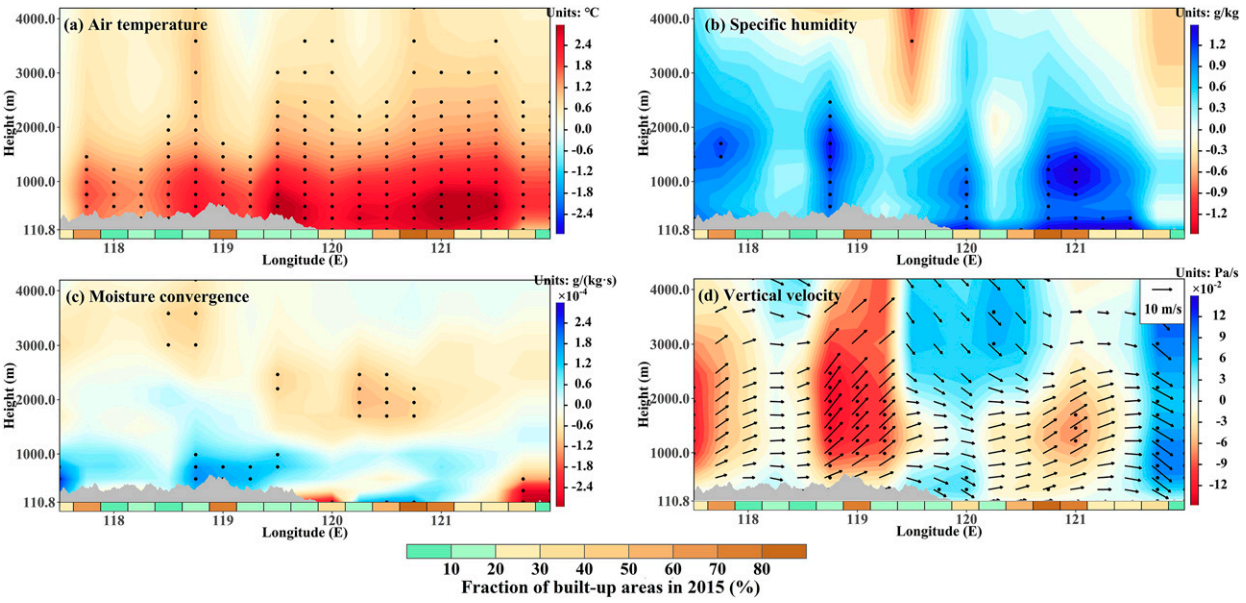

FIG. 8. Impact of urban areas on the vertical structure of the atmosphere. Vertical transect along 30.0°–30.6°N of mean differences in (a) air temperature, (b) specific humidity, (c) moisture convergence, and (d) vertical velocity at multiple layers between the 1 day prior to HW-preceded HP events and the 1 day prior to NoHW-preceded HP events during the period 2000–19 with the highest urbanization. Daily values of multilayer air temperature, specific humidity, moisture convergence, and vertical velocity are obtained from the ERA5 reanalysis data. All NoHW-preceded HP events and HW-preceded HP events are identified using in situ daily observations at the 115 stations across the YRD. For each ERA5 grid in this meridional belt (i.e., the 30.0°–30.6°N transect), we match this grid with its nearest station and match the NoHW-preceded HP events and HW-preceded HP events identified in this station with this ERA5 grid. In (a), we extract multilayer values of air temperature in the one day prior to HW-preceded (NoHW-preceded) HP events to form series 1 (2), and calculate the difference of mean value between series 1 and 2 [i.e., mean (series 1) minus mean (series 2)]; the black dots in (a) indicate the difference between series 1 and 2 is significant at the 90% confidence level. (b)–(d) As in (a), but for specific humidity, moisture convergence, and vertical velocity, respectively. In (d), vectors are differences in zonal wind and vertical velocity between the 1 day prior to HW-preceded HP events and the 1 day prior to NoHW-preceded HP events along the cross section. Gray polygons in each panel indicate topography, and the bottom bars show the fraction of built-up areas (estimated in the year 2015) in each longitude grid along the cross section.

of HWs and urbanization on the increases in the four HP characteristics.

We further create vertical profiles of the atmosphere along a 30.0°–30.6°N transect (because of this meridional belt located in the middle of the YRD and through the core metropolitan areas) of differences in air temperature, specific humidity, moisture convergence, and vertical wind speed at multiple layers between the 1 day prior to HW-preceded HP events and the 1 day prior to NoHW-preceded HP events during the more urbanized period 2000–19 (Fig. 8; see for 2 days and 3 days prior to these events in Figs. S7 and S8). A strong surface temperature perturbation occurs across the whole profile and is most prominent above the urban areas (Fig. 8a), which are responsible for the enhancement of atmospheric instability. More moisture occurs in the low–middle atmosphere above the urban areas (Fig. 8b), together with an intense ascending motion (Fig. 8d), low-level moisture convergence, and upper-level moisture divergence (Fig. 8c). More available moisture and stronger moisture convergence over the urban areas further confirm that HWs favor more intense HP events in urban areas.

These changes in large-scale environmental conditions are usually associated with UHI effects (Li et al. 2020; P. Yang et al. 2017; Zhang et al. 2017). Therefore, we investigate whether there are differences in UHI intensity between the 1 day prior to HW-preceded HP events and the 1 day prior to NoHW-preceded HP events (Fig. 9a). We find that UHI intensity is clearly enhanced under HWs compared to no-HW conditions before HP events, revealing synergistic interactions between UHI and HWs, which have also been reported in previous studies (Li and Bou-Zeid 2013; Li et al. 2015; Zong et al. 2021). On the one hand, stronger negative relations between UHI intensity and near-surface wind speed in urban areas are found for HW-preceded than for NoHW-preceded HP events (Fig. 9b), and lower wind speed under HWs can reduce advective cooling from rural areas (Wang et al. 2017). On the other hand, according to the surface energy budget $R_n + \mathrm{AH} = H + \mathrm{LE} + G$ (where R_n is the net radiation determined by net short- and longwave radiation, AH is the anthropogenic heat flux, H is the surface sensible heat flux, LE is the surface latent heat flux, and G is the heat flux into the ground or buildings; Bateni and Entekhabi 2012; Li and Bou-Zeid 2013; Li et al. 2015; Zong et al. 2021), urban areas receive more net radiation, especially net shortwave radiation during HWs, while the radiative energy input into urban areas

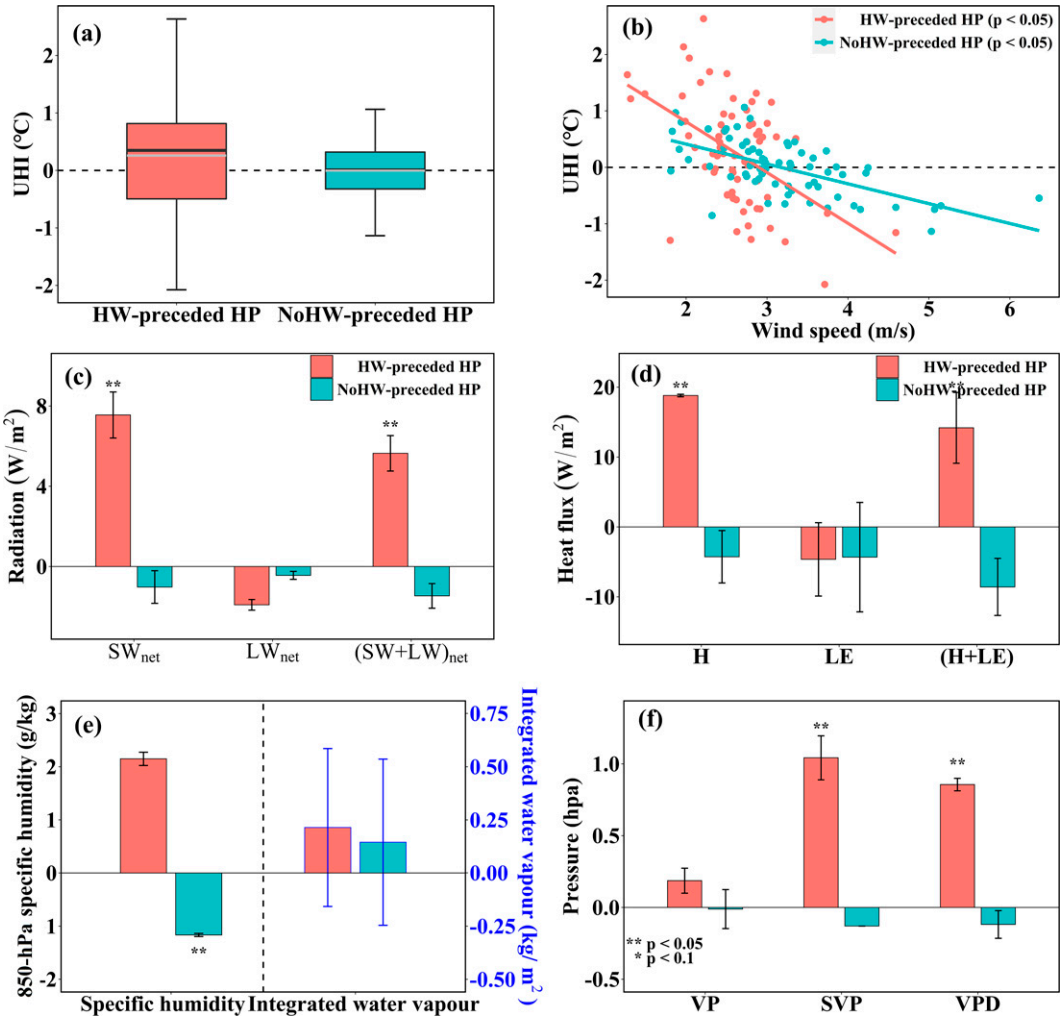

FIG. 9. (a)–(f) Synergistic effects of HWs and UHI on HW-preceded HP events in urban areas of the YRD region during the summer season of 1961–2019. In (a)–(e), daily near-surface air temperature, near-surface wind speed, surface net shortwave radiation flux SW_{net} and surface net longwave radiation flux LW_{net}, surface sensible heat flux H and surface latent heat flux LE, 850-hPa specific humidity, and integrated water vapor are obtained from the ERA5 reanalysis data. In (f), near-surface VP, near-surface SVP, and near-surface VPD are estimated based on the in situ daily observations at the 115 stations across the YRD. All NoHW-preceded HP events and HW-preceded HP events are identified using in situ daily observations at the 115 stations across the YRD. If one of the 115 stations is located at an ERA5 grid, we match daily values of the above variables [see (a)–(e)] in this ERA5 grid with this station. For each of the 68 urban stations, we pair this urban station with its nearest rural station. In (a), the difference in near-surface air temperature in the one day prior to HW-preceded (NoHW-preceded) HP events between the urban stations and paired rural stations, i.e., the UHI intensity, is shown in red (blue) boxplot. In (b), the same as the near-surface air temperature, we calculate the difference in near-surface wind speed, which is plotted by the UHI intensity (each red/blue dot indicates one urban station). Panels (c)–(f) are as in (a), but for SW_{net}, LW_{net}, and total net radiation $(SW + LW)_{net}$ in (c); H, LE, and available energy (H + LE) in (d); 850-hPa specific humidity and integrated water vapor in (e); and VP, SVP, and VPD in (f). Bar plots in (c)–(f) are the mean of the difference for all the 68 urban stations, error bars indicate the corresponding 25%–75% uncertainty intervals, and ** (*) indicates the difference is significant at the 95% (90%) confidence level.

is lower than into rural areas for NoHW-preceded HP events (Fig. 9c). As a result, surface sensible heat flux and available energy show a positive (negative) urban–rural contrast for HW-preceded (NoHW-preceded) HP events (Fig. 9d). The contrasting responses of the surface energy budget also explain the stronger UHI intensity in the days prior to HW-preceded HP events. These results are not sensitive to the choice of 1, 2, and 3 day(s) prior to HP events (Figs. S9 and S10).

The anthropogenic heat flux is defined as "the heat converted from consumption of biological, chemical and electrical

energy and released to the atmosphere due to human activities" (Liu et al. 2022, p. 4721). The AH value is usually obviously larger in urban areas than in the surrounding rural areas, which positively contributes to the UHI intensity (Sailor 2011; Li et al. 2015). During HWs, the increased demand of water and electricity for cooling in cities can enlarge the AH difference between urban and rural areas, resulting in stronger UHI intensity (Zong et al. 2021). However, it is a great challenge to quantify the effects of AH on the UHI due to lacking specific AH data (Chow et al. 2014; Nie et al. 2014).

The synergistic effects of HWs and UHI on HW-preceded HP events are usually associated with local-scale weather systems, which are mainly controlled by thermal effects. We observe a positive urban–rural contrast in 850-hPa specific humidity for HW-preceded HP events, as well as a positive contrast in near-surface vapor pressure (VP), saturated vapor pressure (SVP), and vapor pressure deficit (VPD; Figs. 9e,f). However, the urban–rural contrast is negative for NoHW-preceded HP events. In this study, daily mean near-surface air temperature is included to identify HWs. Actually, HWs can be identified based on daytime and/or nighttime hot extremes. Previous studies found that compound HWs (i.e., co-occurring daytime and nighttime hot extremes on the same day) increase substantially in China during the past decades, mainly due to the significant increases in nighttime HWs (Chen and Zhai 2017; Wu et al. 2021). Urbanization contributes larger to the increases in compound HWs than the increases in daytime HWs (Ma and Yuan 2021; Wang et al. 2021). Increases in compound HWs indicate both higher daytime and nighttime air temperature in urban areas, resulting in more persistent UHI intensity. On the other hand, increases in nighttime air temperature over the YRD is mainly driven by downward longwave radiation, which is linked to increases in atmospheric humidity (transported from the oceans due to an anticyclonic anomaly over the South China Sea; Luo et al. 2022). More persistent UHI intensity and higher atmospheric humidity during compound HWs can provide more favorable environmental conditions for the subsequent HP formation in urban areas.

There is no obvious difference in the urban–rural contrast of integrated water vapor between HW-preceded and NoHW-preceded HP events, indicating a limited influence of the UHI on external moisture transport. Nevertheless, the lower wind speed in areas with a greater UHI effect (Fig. 9b) could favor the longer residence times of local stormy weather systems over urban areas and prolong HP events (Bornstein and Lin 2000). For NoHW-preceded HP events, large-scale weather systems that are mainly controlled by dynamic effects may play a more important role in their occurrences and changes (Ng et al. 2021). HP events produced by large-scale weather systems tend to experience HP stalling over large spatial extents (such as the recording-breaking mei-yu precipitation in 2020; Liu et al. 2020), with front systems and meridional circulation (Ng et al. 2021; Ding et al. 2020), while the impacts of HWs and urban effects may be relatively less important.

4. Conclusions

This work explores the role of moist heatwaves in driving heavy precipitation over urban areas by using long-term daily meteorological observations at 115 stations during the summer season of 1961–2019 in a highly urban region, the Yangtze River delta. During the past six decades, the YRD witnessed increasing frequency, duration, maximum intensity, and cumulative intensity of HP events, with the most prominent increases over urban areas. We find the rapid urbanization of the YRD indeed amplified increases in the four HP characteristics in urban areas, with estimated contributions to the increases of frequency, duration, maximum intensity, and cumulative intensity of 34.25%, 37.50%, 24.62%, and 22.66%, respectively. We only observe these urban effects in HW-preceded HP events (i.e., HWs occurring within the 3 days prior to a HP event), while the urban effects in NoHW-preceded HP events are absent or very weak. These results indicate that HWs play a key role in magnifying the effects of urbanization-induced increases in HP over urban areas of the YRD region.

The back-to-back occurrences of HWs and HP events have been widely reported in recent years (Wang et al. 2019; Zhang and Villarini 2020; Chen et al. 2021; You and Wang 2021; Gu et al. 2022; Li et al. 2022; Ning et al. 2022). Chen et al. (2021) expounded the causality between HWs and HP events in southern China (including the YRD region): 1) the alternative occurrences of wandering subtropical jets and tropical intraseasonal oscillations (Li and Zhou 2013; Chen and Zhai 2017) could trigger the sequential hot and stormy days; 2) tropical cyclones are likely to indirectly and/or directly promote the formation of HWs (Parker et al. 2013; Matthews et al. 2019) and trigger HP events (Q. Zhang et al. 2018; Lai et al. 2020, 2021), hence as an intermediary for the lagged occurrences of HWs and HP events; and 3) more uneven intra-annual distribution of precipitation (Pendergrass and Knutti 2018) and prolonged hot–dry days (Ye and Fetzer 2019; C. X. Li et al. 2021) can increase the probability of HWs encountering sequential HP events.

In the YRD region, about 16.4% of summer HP events are associated with tropical cyclones (Jiang et al. 2020). Besides tropical cyclones, the East Asian summer monsoon (EASM) carries abundant water vapor to produce HP events in summer, which is usually called mei-yu in China, and these HP events are usually linked to the synoptic-scale mei-yu front (Ding et al. 2020). During HWs, surface sensible heat flux is enhanced, atmospheric moisture is accumulated, atmospheric instability is increased, and low-level moisture convergence is strengthened [also see Zhang and Villarini (2020) and You and Wang (2021)]. These enhanced processes are more prominent in urban areas than in rural areas. The enlarged demand of atmospheric water vapor in urban areas under HWs can be supplemented by the EASM (i.e., southerly wind brings moisture from oceans to the YRD region when the mei-yu front stays over this region). The increased atmospheric instability and enhanced moisture convergence under HWs in urban areas can provide favorable synoptic preconditions for sequential HP formation in the mei-yu system. The quantified

evidence for the relationship between HWs, mei-yu front, and HP events should be further investigated by numerical simulation, which is beyond the scope of this study.

On the other hand, during HWs, urban areas receive more net radiation, especially net shortwave radiation, than rural areas. This leads to higher available energy, especially surface sensible heat flux, in urban areas than the surrounding rural areas, resulting in stronger UHI intensity. The strengthening of UHI may further drive atmosphere instability and enhance low-level horizontal convergence in urban areas, leading to increases in HP. The amplification effects of UHI on HP have been widely investigated in previous studies (Gao et al. 2021; Yu et al. 2022). Low wind speed during HWs in urban areas not only can reduce the cooling advection from rural areas [i.e., enhance the synergistic interactions between UHI and HWs; also see Li and Bou-Zeid (2013) and Zong et al. (2021)] but also can favor the longer residence times of local stormy weather systems over urban areas. These synergistic interactions between UHI and HWs can further magnify the amplification effects of urbanization on HP in urban areas. Our findings thus reveal that the amplification effects of urbanization on HP occurs mainly in HW-preceded HP events, suggesting that there is a need for further research into the effects of moist HWs in the urban water cycle.

Acknowledgments. We acknowledge the following projects to support this study: the National Natural Science Foundation of China (Grants U1911205 and 41901041), the China National Key R&D Program (Grant 2018YFA0605603), the open funding from State Key Laboratory of Water Resources and Hydropower Engineering Science (Wuhan University; Grant 2021SWG01), the Central Educational Reform Fund for Colleges and Universities (Grant 2020G12), and the Fundamental Research Funds for the Central Universities, China University of Geosciences (Wuhan; CUG170103). X. Gu is also supported by the China Scholarship Council. L. S. is supported by UKRI (MR/V022008/1). C. Li is supported by the Innovation and Entrepreneurship Training Program for College Students (Grant 202110491010). We thank the three reviewers for their suggestions and comments. X. Gu and D. Kong designed this study. C. Li and X. Gu analyzed data and wrote the first draft of this paper. All authors contributed to the analysis, explaining the results, and editing the final draft. The authors declare that they have no competing interests.

Data availability statement. Station-based meteorological observations were obtained from the National Meteorological Science Data Center at http://www.nmic.cn/en. Original daily values are not available for public download, but we provide all the processed values associated with our results at https://doi.org/10.5281/zenodo.5174963. The land-use/land-cover dataset is available at https://zenodo.org/record/3923728#.Xv1plZMzZs9. The ERA5 reanalysis data are available at https://www.ecmwf.int/en/forecasts/datasets/reanalysis-datasets/era5. All codes related to our results are available from the corresponding author (Xihui Gu) on reasonable request.

REFERENCES

Ali, H., H. J. Fowler, G. Lenderink, E. Lewis, and D. Pritchard, 2021: Consistent large-scale response of hourly extreme precipitation to temperature variation over land. *Geophys. Res. Lett.*, **48**, e2020GL090317, https://doi.org/10.1029/2020GL090317.

Bassett, R., V. Janes-Bassett, J. Phillipson, P. J. Young, and G. S. Blair, 2021: Climate driven trends in London's urban heat island intensity reconstructed over 70 years using a generalized additive model. *Urban Climate*, **40**, 100990, https://doi.org/10.1016/j.uclim.2021.100990.

Bateni, S. M., and D. Entekhabi, 2012: Relative efficiency of land surface energy balance components. *Water Resour. Res.*, **48**, W04510, https://doi.org/10.1029/2011WR011357.

Bornstein, R., and Q. Lin, 2000: Urban heat island and summertime convective thunderstorms in Atlanta: Three case studies. *Atmos. Environ.*, **34**, 507–516, https://doi.org/10.1016/S1352-2310(99)00374-X.

Chen, H., and J. Sun, 2017: Contribution of human influence to increased daily precipitation extremes over China. *Geophys. Res. Lett.*, **44**, 2436–2444, https://doi.org/10.1002/2016GL072439.

Chen, Y., and P. M. Zhai, 2017: Revisiting summertime hot extremes in China during 1961–2015: Overlooked compound extremes and significant changes. *Geophys. Res. Lett.*, **44**, 5096–5103, https://doi.org/10.1002/2016GL072281.

——, Z. Liao, Y. Shi, Y. Tian, and P. Zhai, 2021: Detectable increases in sequential flood-heatwave events across China during 1961–2018. *Geophys. Res. Lett.*, **48**, e2021GL092549, https://doi.org/10.1029/2021GL092549.

Chow, W. T. L., F. Salamanca, M. Georgescu, A. Mahalov, J. M. Milne, and B. L. Ruddell, 2014: A multi-method and multi-scale approach for estimating city-wide anthropogenic heat fluxes. *Atmos. Environ.*, **99**, 64–76, https://doi.org/10.1016/j.atmosenv.2014.09.053.

Dai, A. G., T. B. Zhao, and J. Chen, 2018: Climate change and drought: A precipitation and evaporation perspective. *Curr. Climate Change Rep.*, **4**, 301–312, https://doi.org/10.1007/s40641-018-0101-6.

Ding, Y., P. Liang, Y. Liu, and Y. Zhang, 2020: Multiscale variability of meiyu and its prediction: A new review. *J. Geophys. Res. Atmos.*, **125**, e2019JD031496, https://doi.org/10.1029/2019JD031496.

Fischer, E. M., and C. Schar, 2010: Consistent geographical patterns of changes in high-impact European heatwaves. *Nat. Geosci.*, **3**, 398–403, https://doi.org/10.1038/ngeo866.

Freitag, B. M., U. S. Nair, and D. Niyogi, 2018: Urban modification of convection and rainfall in complex terrain. *Geophys. Res. Lett.*, **45**, 2507–2515, https://doi.org/10.1002/2017GL076834.

Gao, H. Y., Y. L. Luo, X. L. Jiang, D. L. Zhang, Y. Chen, Y. Q. Wang, and X. Y. Shen, 2021: A statistical analysis of extreme hot characteristics and their relationships with urbanization in southern China during 1971–2020. *J. Appl. Meteor. Climatol.*, **60**, 1301–1317, https://doi.org/10.1175/JAMC-D-21-0012.1.

Giorgi, F., E. S. Im, E. Coppola, N. S. Diffenbaugh, X. J. Gao, L. Mariotti, and Y. Shi, 2011: Higher hydroclimatic intensity with global warming. *J. Climate*, **24**, 5309–5324, https://doi.org/10.1175/2011JCLI3979.1.

Gu, L., and Coauthors, 2022: Global increases in compound flood-hot extreme hazards under climate warming. *Geophys. Res. Lett.*, **49**, e2022GL097726, https://doi.org/10.1029/2022GL097726.

Gu, X., Q. Zhang, J. Li, V. P. Singh, and P. Sun, 2019a: Impact of urbanization on nonstationarity of annual and seasonal

precipitation extremes in China. *J. Hydrol.*, **575**, 638–655, https://doi.org/10.1016/j.jhydrol.2019.05.070.

——, ——, V. P. Singh, C. Song, P. Sun, and J. Li, 2019b: Potential contributions of climate change and urbanization to precipitation trends across China at national, regional and local scales. *Int. J. Climatol.*, **39**, 2998–3012, https://doi.org/10.1002/joc.5997.

Hamed, K. H., and A. R. Rao, 1998: A modified Mann-Kendall trend test for autocorrelated data. *J. Hydrol.*, **204**, 182–196, https://doi.org/10.1016/S0022-1694(97)00125-X.

Hersbach, H., and Coauthors, 2020: The ERA5 global reanalysis. *Quart. J. Roy. Meteor. Soc.*, **146**, 1999–2049, https://doi.org/10.1002/qj.3803.

Jiang, X., Y. Luo, D.-L. Zhang, and M. Wu, 2020: Urbanization enhanced summertime extreme hourly precipitation over the Yangtze River delta. *J. Climate*, **33**, 5809–5826, https://doi.org/10.1175/JCLI-D-19-0884.1.

Kong, D., X. Gu, J. Li, G. Ren, and J. Liu, 2020: Contributions of global warming and urbanization to the intensification of human-perceived heatwaves over China. *J. Geophys. Res. Atmos.*, **125**, e2019JD032175, https://doi.org/10.1029/2019JD032175.

Lai, Y. C., and Coauthors, 2020: Greater flood risks in response to slowdown of tropical cyclones over the coast of China. *Proc. Natl. Acad. Sci. USA*, **117**, 14 751–14 755, https://doi.org/10.1073/pnas.1918987117.

——, J. F. Li, X. H. Gu, Y. D. Chen, C. C. Liu, and Y. D. Chen, 2021: Global compound floods from precipitation and storm surge: Hazards and the roles of cyclones. *J. Climate*, **34**, 8319–8339, https://doi.org/10.1175/JCLI-D-21-0050.1.

Li, C. X., X. H. Gu, W. K. Bai, L. J. Slater, J. F. Li, D. D. Kong, J. Y. Liu, and Y. A. Li, 2021: Asymmetric response of short- and long-duration dry spells to warming during the warm-rain season over eastern monsoon China. *J. Hydrol.*, **603**, 127114, https://doi.org/10.1016/j.jhydrol.2021.127114.

——, and Coauthors, 2022: Substantial increase in heavy precipitation events preceded by moist heatwaves over China during 1961–2019. *Front. Environ. Sci.*, **10**, 951392, https://doi.org/10.3389/fenvs.2022.951392.

Li, D., and E. Bou-Zeid, 2013: Synergistic interactions between urban heat islands and heat waves: The impact in cities is larger than the sum of its parts. *J. Appl. Meteor. Climatol.*, **52**, 2051–2064, https://doi.org/10.1175/JAMC-D-13-02.1.

——, T. Sun, M. Liu, L. Yang, L. Wang, and Z. Gao, 2015: Contrasting responses of urban and rural surface energy budgets to heat waves explain synergies between urban heat islands and heat waves. *Environ. Res. Lett.*, **10**, 054009, https://doi.org/10.1088/1748-9326/10/5/054009.

Li, J., Y. D. Chen, T. Y. Gan, and N.-C. Lau, 2018: Elevated increases in human-perceived temperature under climate warming. *Nat. Climate Change*, **8**, 43–47, https://doi.org/10.1038/s41558-017-0036-2.

Li, R. C. Y., and W. Zhou, 2013: Modulation of western North Pacific tropical cyclone activity by the ISO. Part I: Genesis and intensity. *J. Climate*, **26**, 2904–2918, https://doi.org/10.1175/JCLI-D-12-00210.1.

Li, Y., and Coauthors, 2020: Strong intensification of hourly rainfall extremes by urbanization. *Geophys. Res. Lett.*, **47**, e2020GL088758, https://doi.org/10.1029/2020GL088758.

——, W. Wang, M. Chang, and X. Wang, 2021: Impacts of urbanization on extreme precipitation in the Guangdong–Hong Kong–Macau Greater Bay Area. *Urban Climate*, **38**, 100904, https://doi.org/10.1016/j.uclim.2021.100904.

Liang, P., and Y. Ding, 2017: The long-term variation of extreme heavy precipitation and its link to urbanization effects in Shanghai during 1916–2014. *Adv. Atmos. Sci.*, **34**, 321–334, https://doi.org/10.1007/s00376-016-6120-0.

Liao, W., and Coauthors, 2018: Stronger contributions of urbanization to heat wave trends in wet climates. *Geophys. Res. Lett.*, **45**, 11 310–11 317, https://doi.org/10.1029/2018GL079679.

Liao, Z., Y. Chen, W. Li, and P. M. Zhai, 2021: Growing threats from unprecedented sequential flood-hot extremes across China. *Geophys. Res. Lett.*, **48**, e2021GL094505, https://doi.org/10.1029/2021GL094505.

Liu, B., Y. Yan, C. Zhu, S. Ma, and J. Li, 2020: Record-breaking meiyu rainfall around the Yangtze River in 2020 regulated by the subseasonal phase transition of the North Atlantic Oscillation. *Geophys. Res. Lett.*, **47**, e2020GL090342, https://doi.org/10.1029/2020GL090342.

Liu, Y. Q., Z. W. Luo, and S. Grimmond, 2022: Revising the definition of anthropogenic heat flux from buildings: Role of human activities and building storage heat flux. *Atmos. Chem. Phys.*, **22**, 4721–4735, https://doi.org/10.5194/acp-22-4721-2022.

Lu, C., F. C. Lott, Y. Sun, P. A. Stott, and N. Christidis, 2020: Detectable anthropogenic influence on changes in summer precipitation in China. *J. Climate*, **33**, 5357–5369, https://doi.org/10.1175/JCLI-D-19-0285.1.

Lu, M., Y. Xu, N. Shan, Q. Wang, J. Yuan, and J. Wang, 2019: Effect of urbanisation on extreme precipitation based on nonstationary models in the Yangtze River delta metropolitan region. *Sci. Total Environ.*, **673**, 64–73, https://doi.org/10.1016/j.scitotenv.2019.03.413.

Luo, M., and N.-C. Lau, 2018: Increasing heat stress in urban areas of eastern China: Acceleration by urbanization. *Geophys. Res. Lett.*, **45**, 13 060–13 069, https://doi.org/10.1029/2018GL080306.

——, and ——, 2019: Urban expansion and drying climate in an urban agglomeration of East China. *Geophys. Res. Lett.*, **46**, 6868–6877, https://doi.org/10.1029/2019GL082736.

——, and ——, 2021: Increasing human-perceived heat stress risks exacerbated by urbanization in China: A comparative study based on multiple metrics. *Earth's Future*, **9**, e2020EF001848, https://doi.org/10.1029/2020EF001848.

——, ——, and Z. Liu, 2022: Different mechanisms for daytime, nighttime, and compound heatwaves in southern China. *Wea. Climate Extremes*, **36**, 100449, https://doi.org/10.1016/j.wace.2022.100449.

Ma, F., and X. Yuan, 2021: More persistent summer compound hot extremes caused by global urbanization. *Geophys. Res. Lett.*, **48**, e2021GL093721, https://doi.org/10.1029/2021GL093721.

Ma, S., and Coauthors, 2017: Detectable anthropogenic shift toward heavy precipitation over eastern China. *J. Climate*, **30**, 1381–1396, https://doi.org/10.1175/JCLI-D-16-0311.1.

Massey, F. J., 1951: The Kolmogorov-Smirnov test for goodness of fit. *J. Amer. Stat. Assoc.*, **46**, 68–78, https://doi.org/10.1080/01621459.1951.10500769.

Matthews, T., R. L. Wilby, and C. Murphy, 2019: An emerging tropical cyclone-deadly heat compound hazard. *Nat. Climate Change*, **9**, 602–606, https://doi.org/10.1038/s41558-019-0525-6.

Mazdiyasni, O., and A. AghaKouchak, 2015: Substantial increase in concurrent droughts and heatwaves in the United States. *Proc. Natl. Acad. Sci. USA*, **112**, 11 484–11 489, https://doi.org/10.1073/pnas.1422945112.

Meili, N., A. Paschalis, G. Manoli, and S. Fatichi, 2022: Diurnal and seasonal patterns of global urban dry islands. *Environ.*

Res. Lett., **17**, 054044, https://doi.org/10.1088/1748-9326/ac68f8.

Ng, C.-P., Q. Zhang, and W. Li, 2021: Changes in hourly extreme precipitation over eastern China from 1970 to 2019 dominated by synoptic-scale precipitation. *Geophys. Res. Lett.*, **48**, e2020GL090620, https://doi.org/10.1029/2020GL090620.

Nie, W. S., T. Sun, and G. H. Ni, 2014: Spatiotemporal characteristics of anthropogenic heat in an urban environment: A case study of Tsinghua Campus. *Build. Environ.*, **82**, 675–686, https://doi.org/10.1016/j.buildenv.2014.10.011.

Ning, G. C., M. Luo, W. Zhang, Z. Liu, S. G. Wang, and T. Gao, 2022: Rising risks of compound extreme heat-precipitation events in China. *Int. J. Climatol.*, **42**, 5785–5795, https://doi.org/10.1002/joc.7561.

Nogueira, M., A. Hurduc, S. Ermida, D. C. A. Lima, P. M. M. Soares, F. Johannsen, and E. Dutra, 2022: Assessment of the Paris urban heat island in ERA5 and offline SURFEX-TEB (v8.1) simulations using the METEOSAT land surface temperature product. *Geosci. Model Dev.*, **15**, 5949–5965, https://doi.org/10.5194/gmd-15-5949-2022.

Parker, T. J., G. J. Berry, and M. J. Reeder, 2013: The influence of tropical cyclones on heat waves in southeastern Australia. *Geophys. Res. Lett.*, **40**, 6264–6270, https://doi.org/10.1002/2013GL058257.

Pendergrass, A. G., and R. Knutti, 2018: The uneven nature of daily precipitation and its change. *Geophys. Res. Lett.*, **45**, 11 980–11 988, https://doi.org/10.1029/2018GL080298.

Qian, Y., and Coauthors, 2022: Urbanization impact on regional climate and extreme weather: Current understanding, uncertainties, and future research directions. *Adv. Atmos. Sci.*, **39**, 819–860, https://doi.org/10.1007/s00376-021-1371-9.

Ren, G., Y. Zhou, Z. Chu, J. Zhou, A. Zhang, J. Guo, and X. Liu, 2008: Urbanization effects on observed surface air temperature trends in North China. *J. Climate*, **21**, 1333–1348, https://doi.org/10.1175/2007JCLI1348.1.

Sailor, D. J., 2011: A review of methods for estimating anthropogenic heat and moisture emissions in the urban environment. *Int. J. Climatol.*, **31**, 189–199, https://doi.org/10.1002/joc.2106.

Shi, Z. T., X. Y. Xu and G. S. Jia, 2021: Urbanization magnified nighttime heat waves in China. *Geophys. Res. Lett.*, **48**, e2021GL093603, https://doi.org/10.1029/2021GL093603.

Song, X. M., Y. C. Mo, Y. Q. Xuan, Q. J. Wang, W. Y. Wu, J. Y. Zhang, and X. J. Zou, 2021: Impacts of urbanization on precipitation patterns in the greater Beijing-Tianjin-Hebei metropolitan region in northern China. *Environ. Res. Lett.*, **16**, 014042, https://doi.org/10.1088/1748-9326/abd212.

Tan, X. Z., and T. Y. Gan, 2017: Non-stationary analysis of the frequency and intensity of heavy precipitation over Canada and their relations to large-scale climate patterns. *Climate Dyn.*, **48**, 2983–3001, https://doi.org/10.1007/s00382-016-3246-9.

Tysa, S. K., G. Y. Ren, Y. Qin, P. F. Zhang, Y. Y. Ren, W. Q. Jia, and K. M. Wen, 2019: Urbanization effect in regional temperature series based on a remote sensing classification scheme of stations. *J. Geophys. Res. Atmos.*, **124**, 10 646–10 661, https://doi.org/10.1029/2019JD030948.

Venter, Z. S., T. Chakraborty, and X. H. Lee, 2021: Crowdsourced air temperatures contrast satellite measures of the urban heat island and its mechanisms. *Sci. Adv.*, **7**, eabb9569, https://doi.org/10.1126/sciadv.abb9569.

Wang, J., Z. Yan, X.-W. Quan, and J. Feng, 2017: Urban warming in the 2013 summer heat wave in eastern China. *Climate Dyn.*, **48**, 3015–3033, https://doi.org/10.1007/s00382-016-3248-7.

——, J. M. Feng, and Z. W. Yan, 2018: Impact of extensive urbanization on summertime rainfall in the Beijing region and the role of local precipitation recycling. *J. Geophys. Res. Atmos.*, **123**, 3323–3340, https://doi.org/10.1002/2017JD027725.

——, and Coauthors, 2021: Anthropogenic emissions and urbanization increase risk of compound hot extremes in cities. *Nat. Climate Change*, **11**, 1084–1089, https://doi.org/10.1038/s41558-021-01196-2.

Wang, Jie, F. Chen, Q.-V. Doan, and Y. Xu, 2021: Exploring the effect of urbanization on hourly extreme rainfall over Yangtze River delta of China. *Urban Climate*, **36**, 100781, https://doi.org/10.1016/j.uclim.2021.100781.

Wang, P., and Coauthors, 2022: Amplification effect of urbanization on atmospheric aridity over China under past global warming. *Earth's Future*, **10**, e2021EF002335, https://doi.org/10.1029/2021EF002335.

Wang, S. S.-Y., H. Kim, D. Coumou, J.-H. Yoon, L. Zhao, and R. R. Gillies, 2019: Consecutive extreme flooding and heat wave in Japan: Are they becoming a norm? *Atmos. Sci. Lett.*, **20**, e933, https://doi.org/10.1002/asl.933.

Wouters, H., and Coauthors, 2017: Heat stress increase under climate change twice as large in cities as in rural areas: A study for a densely populated midlatitude maritime region. *Geophys. Res. Lett.*, **44**, 8997–9007, https://doi.org/10.1002/2017GL074889.

Wu, S., and Coauthors, 2021: Increasing compound heat and precipitation extremes elevated by urbanization in South China. *Front. Earth Sci.*, **9**, 636777, https://doi.org/10.3389/feart.2021.636777.

Xu, Y., and Coauthors, 2020: Annual 30-m land use/land cover maps of China for 1980–2015 from the integration of AVHRR, MODIS and Landsat data using the BFAST algorithm. *Sci. China Earth Sci.*, **63**, 1390–1407, https://doi.org/10.1007/s11430-019-9606-4.

Yang, L., J. Smith, and D. Niyogi, 2019: Urban impacts on extreme monsoon rainfall and flooding in complex terrain. *Geophys. Res. Lett.*, **46**, 5918–5927, https://doi.org/10.1029/2019GL083363.

——, G. H. Ni, F. Q. Tian, and D. Niyogi, 2021: Urbanization exacerbated rainfall over European suburbs under a warming climate. *Geophys. Res. Lett.*, **48**, e2021GL095987, https://doi.org/10.1029/2021GL095987.

Yang, P., G. Ren, and P. Yan, 2017: Evidence for a strong association of short-duration intense rainfall with urbanization in the Beijing urban area. *J. Climate*, **30**, 5851–5870, https://doi.org/10.1175/JCLI-D-16-0671.1.

Yang, X., L. R. Leung, N. Zhao, C. Zhao, Y. Qian, K. Hu, X. Liu, and B. Chen, 2017: Contribution of urbanization to the increase of extreme heat events in an urban agglomeration in East China. *Geophys. Res. Lett.*, **44**, 6940–6950, https://doi.org/10.1002/2017GL074084.

Ye, H. C., and E. J. Fetzer, 2019: Asymmetrical shift toward longer dry spells associated with warming temperatures during Russian summers. *Geophys. Res. Lett.*, **46**, 11 455–11 462, https://doi.org/10.1029/2019GL084748.

You, J., and S. Wang, 2021: Higher probability of occurrence of hotter and shorter heat waves followed by heavy rainfall. *Geophys. Res. Lett.*, **48**, e2021GL094831, https://doi.org/10.1029/2021GL094831.

Yu, X., and Coauthors, 2022: Asymmetrical shift toward less light and more heavy precipitation in an urban agglomeration of East China: Intensification by urbanization. *Geophys. Res. Lett.*, **49**, e2021GL097046, https://doi.org/10.1029/2021GL097046.

Zhang, G. F., and Coauthors, 2022: Rapid urbanization induced daily maximum wind speed decline in metropolitan areas: A case study in the Yangtze River delta (China). *Urban Climate*, **43**, 101147, https://doi.org/10.1016/j.uclim.2022.101147.

Zhang, Q., X. H. Gu, J. F. Li, P. J. Shi, and V. P. Singh, 2018: The impact of tropical cyclones on extreme precipitation over coastal and inland areas of China and its association to ENSO. *J. Climate*, **31**, 1865–1880, https://doi.org/10.1175/JCLI-D-17-0474.1.

Zhang, W., and G. Villarini, 2020: Deadly compound heat stress-flooding hazard across the central United States. *Geophys. Res. Lett.*, **47**, e2020GL089185, https://doi.org/10.1029/2020GL089185.

——, W. Zhang, G. A. Vecchi, and J. A. Smith, 2018: Urbanization exacerbated the rainfall and flooding caused by Hurricane Harvey in Houston. *Nature*, **563**, 384–388, https://doi.org/10.1038/s41586-018-0676-z.

Zhang, Y., S. Miao, Y. Dai, and R. Bornstein, 2017: Numerical simulation of urban land surface effects on summer convective rainfall under different UHI intensity in Beijing. *J. Geophys. Res. Atmos.*, **122**, 7851–7868, https://doi.org/10.1002/2017JD026614.

Zhao, L., and Coauthors, 2021: Global multi-model projections of local urban climates. *Nat. Climate Change*, **11**, 152–157, https://doi.org/10.1038/s41558-020-00958-8.

Zong, L., S. Liu, Y. Yang, G. Ren, M. Yu, Y. Zhang, and Y. Li, 2021: Synergistic influence of local climate zones and wind speeds on the urban heat island and heat waves in the megacity of Beijing, China. *Front. Earth Sci.*, **9**, 673786, https://doi.org/10.3389/feart.2021.673786.